Published in final edited form as:
J Vac Sci Technol B Nanotechnol Microelectron. 2011 ; 29(3): 032001–. doi:10.1116/1.3581102.

Rapid serial prototyping of magnet-tipped attonewton-sensitivity cantilevers by focused ion beam manipulation

Jonilyn G. Longenecker[1], **Eric W. Moore**[1], and **John A. Marohn**[1,*]
[1]Department of Chemistry and Chemical Biology, Cornell University, Ithaca, New York 14853

Abstract

We report a method for rapidly prototyping attonewton-sensitivity cantilevers with custom-fabricated tips, and illustrate the method by preparing tips consisting of a magnetic nanorod overhanging the leading edge of the cantilevers. Micron-long nickel nanorods with widths of 120 to 220 nm were fabricated on silicon chips by e-beam lithography, deposition, and liftoff. Each silicon chip, with its integral nanomagnet, was attached serially to a custom-fabricated attonewton-sensitivity cantilever using focused ion beam manipulation. The magnetic nanorod tips were prepared with and without an alumina capping layer, and the minimum detectable force and tip magnetic moment of the resulting cantilevers was characterized by cantilever magnetometry. Our results indicate that this serial but high yield approach is an effective way to rapidly prepare and characterize magnetic tips for proposed single-electron-spin and single-proton magnetic resonance imaging experiments. The approach also represents a versatile route for affixing essentially any vacuum-compatible sample to the leading edge of an attonewton-sensitivity cantilever.

I. INTRODUCTION

The development of attonewton-sensitivity cantilevers[1,2] has opened up exciting new approaches for characterizing materials. Attonewton-sensitivity cantilevers have been used to detect electron spin resonance[3,4] and nuclear magnetic resonance,[5,6] to observe near-surface dissipation due to dopants in iconductors[7] and dielectric fluctuations in polymers,[8,9] to characterize switching and fluctuations of ferromagnetic domains in individual magnetic nanoparticles[2,10,11] and individual magnetic vortices in superconducting rings,[12] and to measure persistent currents in normal metal rings.[13,14]

These applications require functionalizing the tip of the attonewton-sensitivity cantilever with, for example, a biological sample,[6] a magnetic nanoparticle or nanorod,[2–5,7,10,11] a metal coating,[8,9] or a superconducting ring.[12] A few approaches have been demonstrated for functionalizing the tip of an attonewton-sensitivity cantilever. These include blanket evaporating a metal film on the cantilever's leading edge[1,7–9] or sidewall,[10] or by manually affixing a sample,[4–6] followed in some cases by focussed ion-beam milling.[3,12] Attonewton-sensitivity cantilevers have been batch fabricated with magnetic tips defined near the leading edge of the cantilever using optical[15] and e-beam[2] lithography. Hickman *et al.* recently demonstrated the batch fabrication of 100 nm diameter nickel nanomagnets that overhang the leading edge of an attonewton-sensitivity cantilever.[16] The tip-functionalization approach demonstrated in Ref. 16 overcomes the size- and time limitations of serial attachment and focussed ion beam milling. Moreover, the nanomagnet overhang improves

*Electronic address: jam99@cornell.edu.

This paper was presented at the AVS 57th International Symposium and Exhibition held in Albuquerque, NM, October 17 – 22, 2010.

the spatial separation between trapped charge on the cantilever and electric field fluctuations in the substrate. The resulting batch-fabricated nickel nanorod tips exhibited a record-small force sensitivity of 10 aN at a tip-sample separation of 3 nm.[16]

While the tips fabricated by Hickman *et al.* exhibited record-small force sensitivity near a surface, their fabrication was problematic. In Fig. 1 we present scanning electron microscope (SEM) images of magnets fabricated using the process presented in Fig. 2 of Ref. 16. The nanomagnets were damaged extensively by process incompatibilities during the thirty-eight step (approximately two week) fabrication process, resulting in extremely low yields and in damage layers on intact magnets in excess of 15 nm. Less than 1% of the magnets remained intact (Fig. 1(b)) after processing, whereas most magnets were either completely absent after processing (Fig. 1(c)) or, we surmised, formed a silicide with the underlying silicon substrate and were no longer magnetic (Fig. 1(d)).[17] The mechanism leading to this extensive damage was extremely difficult to explore since, to avoid physical and (it is thought) oxidative damage, the magnets were encased in oxide during backside processing.[1,16]

In order to conduct high resolution magnetic resonance force microscopy (MRFM) experiments, process yields must be greatly improved and the extent of magnet damage must be reduced, particularly at the leading edge where the force gradient acting on the sample spins is greatest. Motivated by the challenge of understanding the magnet damage mechanism, we developed a rapid-prototyping technique for fabricating overhanging magnets on attonewton-sensitivity cantilevers. This approach enables analysis and characterization at essentially any step in the fabrication procedure; reduces the processing time from approximately two weeks to just four days; and completely decouples the fabrication of the nanomagnets, which are particularly susceptible to heating and chemical damage, from the fabrication of the cantilevers, which involves high-temperature reactive-ion etching steps during backside processing.

The first step in our new fabrication technique is the batch fabrication of silicon microchips with integrated, overhanging magnetic nanorods. These microchips are free-standing prior to deposition of the magnets so that the chips can be analyzed after any post-deposition processing step. The magnet-tipped chips are serially attached to separately-fabricated attonewton-sensitivity silicon cantilevers using focused ion beam (FIB) manipulation. FIB manipulation is routinely employed to image sample cross-sections[18,19] and to prepare transmission electron microscopy (TEM) samples.[20–23] Here we show that the ability of FIB to mill, transfer, and adhere samples with microscale precision makes it an ideal tool for lifting out the magnet-tipped chips and adhering them to the leading edge of cantilevers. The resulting magnets overhang the leading edge of the silicon cantilever and should therefore achieve the same exceptional force sensitivity near a surface as Hickman *et al.*'s cantilevers.

In Sec. II we describe our fabrication and FIB attachment protocols. In Sec. III we discuss the measured yield of these processes and the characterization of the magnets and cantilevers via SEM analysis and cantilever magnetometry.[10,11,24] Our main findings are that the magnet-tipped chip fabrication process is high-yield, that the magnets are consistently well-magnetized, and that the cantilevers are not damaged by the FIB process. In Sec. IV we discuss additional advantages of this combination batch- and serial-fabrication technique, which include the ability to switch to magnetic materials which would supply higher field gradients and the freedom to explore magnet encasement protocols.

II. FABRICATION

In order to increase magnet quality and yield, a novel off-cantilever protocol for fabricating nickel nanomagnets that overhang silicon microchips was developed. In this section we describe the attonewton-sensitivity cantilever (Sec. IIA), nanomagnet-tipped chip (Sec. II B), and FIB manipulation (Sec. II C) protocols, as well as variations of the nanomagnet-tipped chip fabrication process (Sec. IID).

A. Attonewton-sensitivity cantilever fabrication

The fabrication scheme for the cantilevers used in this work, Fig. 1(a), is similar to previous protocols.[1,2,16] In brief, the cantilevers were fabricated from silicon-on-insulator (SOI) wafers (with parameters given below in Sec. II B). The cantilever bodies were patterned by photolithography and defined by reactive ion etching. Backside windows were aligned underneath the cantilever bodies and patterned by photolithography, and were subsequently etched by through-wafer Bosch etching. During the backside processing, the cantilever bodies were protected by a layer of plasma enhanced chemical vapor deposited (PECVD) silicon dioxide. The cantilevers were released in buffered oxide etch (BOE), and critical point dried (CPD) to prevent deformation.

B. Nanomagnet-tipped chip protocol

Overhanging nanomagnet-tipped silicon chips were fabricated from silicon-on-insulator (SOI) wafers having a device silicon thickness of 340 nm, a buried oxide (BOX) thickness of 400 nm, and a silicon handle wafer thickness of 500 μm. The device silicon resistivity is 14–22 Ω cm, corresponding to a boron dopant concentration of $6 – 9 \times 10^{14}$ cm^{-3}.

Liftoff alignment marks for three subsequent electron-beam lithography steps were defined in a bilayer of 50 nm of 950,000 molecular weight (MW) (poly)methylmethacrylate (PMMA) on top of 550 nm of 495,000 MW PMMA, and were patterned using either a JEOL JBX9300FS (at 2 nA) or a JEOL JBX6300FS 100 kV (at 1 nA) electron beam (e-beam) lithography system. The marks were deposited by electron-gun evaporation (CVC products SC 4500 evaporator) and consisited of 100 nm of platinum with a 5 nm chromium adhesion layer, deposited at 2.5 Å/sec and 2.0 Å/sec respectively. The resist and excess metal were removed by sonication in a 1:1 solution of methylene chloride (CH_2Cl_2) and acetone.

Slits to define rectangular chip bodies, along with support tabs halfway along the chip length to prevent post-release stiction, were defined in approximately 700 nm of 495,000 MW PMMA and patterned by e-beam lithography. See Fig. 2(a). The device-layer silicon was etched in sulfur hexafluoride and oxygen (SF_6:O_2; Oxford Instruments Plasmalab 80), and the resist was subsequently stripped by sonication in 1:1 CH_2Cl_2:acetone. The chips were released by wet etching the BOX layer in 6:1 buffered oxide etch, followed by soaking the wafer in a water bath and spin drying.

Nickel nanomagnets with widths of 70 nm, 110 nm, and 220 nm (Fig. 2(b)) were patterned by e-beam lithography in a bilayer of 50 nm of 950,000 MW PMMA on 550 nm of 495,000 MW PMMA. The magnets were deposited by electron-gun evaporation; a 5 nm-thick chromium adhesion layer was deposited prior to evaporating the 90 nm-thick magnets, at a rate of 2.0 Å/s and 2.5 Å/s respectively. After a waiting period to allow the chamber to cool to room temperature, the wafer was unloaded and the resist and excess metal were removed by sonication in 1:1 CH_2Cl_2:acetone, followed by spin drying. To protect against post-processing oxidation, some samples were coated with approximately 6 nm of alumina prior to resist removal. The alumina was prepared via atomic layer deposition using trimethlyaluminum and plasma oxygen precursors at 110°C (ALD; Oxford FlexAL).[25,26]

In order to achieve overhanging magnets, as shown in Fig. 2(c), the silicon under the magnet was removed by defining a U-shaped "etch pit" 50 nm from the leading edge of the magnet and etching the silicon using a calibrated isotropic etch.[16] Simultaneously, the leading edge of the chip rod is removed, providing a well-defined chip leading edge. The etch pit is patterned by e-beam lithography in approximately 700 nm of 495,000 MW PMMA and is etched by a carefully-timed isotropic etch in SF_6:O_2. After the etch, a silicon "finger" is defined at the leading edge of the chip that is 2 to 5 μm long and has a reduced width of 1 μm. The magnets overhang this finger by 300 to 400 nm. The resist was removed by sonication in 1:1 CH_2Cl_2:acetone, followed by spin drying.

Overall, the magnet-tipped silicon chip fabrication protocol requires 17 steps and can be completed in four days. This factor of three improvement in processing time, compared to the integrated magnet-on-cantilever fabrication protocol of Ref. 16, enables rapid prototyping.

C. Focused ion beam liftout and attachment to cantilevers

FIB processing was conducted on a dual-beam FEI Strata 400 STEM FIB system, with ion beam and e-beam imaging, ion beam milling, and platinum deposition capabilities, as well as a probe with a 1 μm-diameter tip (Omniprobe) for transferring samples. The liftout and attachment process is detailed in Fig. 3, and in order to prevent gallium ion implantation damage, the magnets are off-screen in all ion beam images. The ion beam imaging time of the magnets and the cantilever bodies was carefully limited to less than 3 seconds of total exposure. All ion beam processing was done at 30 kV with a nominal ion beam current of 28 pA.

To attach the overhanging magnet-tipped silicon chip to the probe, the probe tip was first brought into light contact ~5 μm from the base of the chip and adhered to the silicon chip using platinum deposition to join the two components (Fig. 3(a)). For all adhesions, approximately 1 μm of locally deposited platinum was achieved by ion-beam induced decomposition of methylcyclopentadienyl(trimethyl)platinum(IV) precursor gas. The chip base and support tabs were subsequently milled (Fig. 3(b)) and the chip gently raised from the substrate and moved near the cantilever's leading edge.

Before the chip was brought into contact with the cantilever, the chip and cantilever were aligned horizontally by rotating the stage (and mounted cantilever) as needed. The chip was softly brought into contact with the cantilever (Fig. 3(c)). Since the cantilevers naturally bend downward at a slight angle, the probe was retracted slightly to pull the cantilever upwards and improve vertical alignment between the chip and the cantilever. Once the vertical alignment was confirmed, platinum was deposited on the sides of the chip and cantilever to adhere them together (Fig. 3(d)). The probe tip was milled and the probe was lifted away from the cantilever (Fig. 3(e)). Additional platinum-deposited contacts were made along the side and top of the cantilever. The completed chip mounted on the cantilever is shown in Fig. 3(f).

D. Variations on the nanomagnet-tipped chip fabrication protocol

The protocol outlined above involves the fabrication of magnets that were deposited on pre-released silicon chips and subsequently underetched to produce an overhanging magnet. Two alternative procedures were also considered in which 1) the chips were released by HF vapor after the overhanging magnets had been defined and 2) non-overhanging magnets were fabricated near the front edge of the silicon chip. The differences between the three procedures can be understood by considering the SEM images of representative silicon chips

presented in Fig. 4. The nanomagnet in Fig. 4(g) was coated with ALD Al_2O_3, whereas the nanomagnets in Fig. 4(b), Fig. 4(d), and Fig. 4(f) were not capped.

Release of the chips by HF vapor instead of by BOE wet etching was considered in order to increase chip stability during processing. Since nickel has been reported to not be etched by HF vapor,[27] whereas nickel is readily etched by BOE, the chips could be released using HF vapor at the end of the process. The main potential benefits of this approach were device stability during processing and shorter overall processing time (reduced by six steps and 2.25 processing hours) since the etching of the the silicon and the underetching of the magnet could now be accomplished in a single step. The chip and nanomagnet shown in Fig. 4(c,d) were released at a rate of 500 Å/min using HF vapor in nitrogen and ethanol carrier gasses (Primaxx uEtch Single Wafer Process Module).

In order to assess the magnet integrity immediately after deposition, a simplified protocol for preparing *non*-overhanging magnets was developed. The main alteration and benefit in this process was that the silicon chips were defined such that one end was free-standing past the support tabs. After the magnetic material was deposited and the resist liftoff completed, no additional processing steps were required prior to FIB liftout. For this process, the entire chip was defined and etched in one e-beam lithography step, where processing was identical to the processing for the slits in Sec. II B, and subsequently released. See Fig. 4(e-g). Although these chips could not be used in an MRFM experiment to detect magnetic resonance or observe surface noise, cantilever magnetometry could nevertheless be conducted to measure tip magnetization and assess the affect of the underetch step on magnet quality.

III. CHARACTERIZATION

In order to characterize the yield of the overall fabrication process, we separately estimated the yields of the magnet-tipped chip bodies, cantilevers, FIB attachment procedure, and magnets. By analyzing thirteen magnet-tipped silicon chip dies, with each die containing 100 individual magnet-tipped silicon chips, an average magnet-tipped chip body yield was 94.2% ± 6.0% measured. It was determined that in order to achieve high yield, the width of the slits, the width of the support tabs, and the length of the leading-edge silicon finger had to be carefully chosen in order to prevent stiction. The need for support tabs can be seen in Fig. 5(a), which shows 15 μm-long chips without slits snapped into contact with the underlying substrate. The silicon finger at the leading edge incurred stiction and curling (Fig. 5(b)) if it was 5μm long, but was stiction-free without critical point drying for short finger lengths of 2 μm (Fig. 4(a-b)). Slits that were too wide resulted in stiction, whereas slits that were too narrow did not provide room for lateral motion during the FIB liftout procedure. Since stiction occurred in approximately 50% of chips with slit widths of 4 μm and in all chips with slit widths wider than 6 μm, widths of 2 to 3 μm were chosen. Likewise, support tabs that were too narrow also resulted in stiction (Fig. 5(c)), whereas support tabs that were as least 4 μm wide remained stiction-free and did not even require critical-point drying.

The cantilever yield was 90.5%, with 190 out of 210 potential cantilevers remaining intact. Yields for similarly processed wafers have ranged from 50% to 90%. The FIB liftout and attachment procedure yield was 90%, with only one failure out of eleven attempts (caused by a crack in the chip silicon that propagated during liftout). After FIB manipulation, the cantilever quality factors remained high, implying that the cantilevers were not damaged by the FIB processing. Cantilever quality factors were measured between 41,000 and 94,000 at 4.2 K and 10^{-6} mbar , consistent with previously reported values for non-FIB processed cantilevers (Table I).[2,16]

The magnets were analyzed by visual inspection and magnetometry. The nanomagnets were imaged by a scanning electron beam (Zeiss Ultra) in order to determine the yield of intact nickel nanomagnets and check for damage resulting from, for example, silicide formation (Fig. 1(d)). It was determined that both the overhanging nanomagnets on the standard prereleased chips and the nonoverhanging magnets on the control chips were present on nearly 100% of the corresponding chips. We conclude that neither set of magnets showed any appreciable silicide damage since the nickel grain structure was clearby visible (Fig. 4(b)). The nickel nanomagnets on the HF-vapor released chips had approximately 20 nm of nickel missing at the leading edge (Fig. 4(d)), and were not characterized further.

Six nickel nanomagnets were analyzed by cantilever frequency-shift magnetometry.[10,11,16] The magnets had widths of 120 nm and 220 nm and were either non-overhanging or had an overhang of ~300 nm (Table I). Magnetometry experiments were conducted on a custom-built probe operating at $T = 4.2$ K and $P = 10^{-6}$ mbar. Changes in cantilever frequency were measured as an external magnetic field applied along the long axis of the magnet was swept between −4 T and +4 T. Cantilever motion was monitored using a fiber-optic interferometer (wavelength $\lambda = 1310$nm and power $P \sim 3$ μW). During the measurement, the cantilever was forced to self oscillate to an RMS amplitude of ~90 nm by using it as the frequency determining element of a PI-controlled-gain positive feedback circuit that drove a piezoelectic element located under the cantilever base. The cantilever frequency was determined by digitizing the interferometer output and using a software frequency demodulator.[28] Spring constant changes Δk were computed from frequency shifts Δf using $\Delta k = 2k\Delta f/f_0$ with k and f_0 the cantilever spring constant and resonance frequency, respectively. Cantilever dissipation was inferred from either the cantilever ringdown time or by following the gain control of the positive feedback loop. The magnetic moment of the tip magnet was extracted by fitting the spring constant shift versus magnetic field data to[10,11,24]:

$$\frac{\Delta k}{k} = \frac{\mu_{\mathrm{sat}}}{k}\left(\frac{\alpha}{l}\right)^2 \frac{B\Delta B}{B+\Delta B}. \quad (1)$$

with μ_{sat} the saturated magnetic moment, $\alpha = 1.377$ a constant dependent on the cantilever mode shape, l the cantilever length, $B = \mu_0 H$ the applied magnetic field and $\Delta B = \mu_0 \mu_{\mathrm{sat}} \Delta N / V$, where $\Delta N = N_t - N_l$ is the difference in demagnetization factor along the cantilever's thickness and length, respectively. The volume V of the tip magnet was computed from estimates of the magnet's lateral dimensions (obtained from SEM micrographs) and thickness (measured for one representative sample using atomic force microscopy). Fractional cantilever frequency shift as a function of applied magnetic field is shown for the magnet on cantilever C1, which had a 200 nm wide overhanging magnet, in Fig. 6. The parameters μ_{sat} and ΔN were obtained from a nonlinear least-squares fit of the frequency-shift data to Eq. 1, and the tip magnetization $\mu_0 M_{\mathrm{sat}}$ was computed using $\mu_0 M_{\mathrm{sat}} = \mu_0 \mu_{\mathrm{sat}} / V$. Fit results are shown in Table I, and the nominal saturated magnetic moment $\mu_{\mathrm{sat}}^{\mathrm{nominal}}$, which was calculated for fully-magnetized nickel particles of the same measured dimensions, is provided for comparison. For one magnet, indicated in the table, the fit was too poor to accurately obtain all three parameters from the frequency-shift data; in this case, ΔN was calculated from the estimated length and thickness using demagnetization factors obtained by Aharoni for a rectangular prism,[29] and μ_{sat} and V were obtained by fitting.

Analysis indicated that the net magnetization of the 220 nm-wide nanomagnets was significantly higher than for the 120 nm-wide nanomagnets. Two magnets with widths of 120 nm were studied on chips C2 and C3 and were between 47 and 70% magnetized and 37 and 47% magnetized, respectively, when compared to the saturation magnetization of bulk nickel ($\mu_0 M_{\mathrm{sat}} = 0.6$T). In contrast, the four 220 nm-wide nanomagnets were all more than

half magnetized; the average magnetization range was 53 to 73%, and the best-magnetized magnet (on C6) was between 68 and 95% magnetized. No significant differences in magnetization were observed between overhanging (C1-C4) and non-overhanging (C5-C6) magnets, implying that the processing steps required to define and etch the U-shaped “etch pit” did not cause damage to the nickel nanomagnets. The cantilever quality factor was not measured to have a strong dependence on applied magnetic field; representative shifts in an applied field of 5T are reported in Table I.

IV. DISCUSSION AND CONCLUSIONS

The primary result of this study is the demonstration of a high-yield, rapid-prototyping protocol for fabricating well-magnetized nickel nanorods on silicon chips and serially attaching them to the leading edge of attonewton-sensitivity cantilevers. Since the magnet chip fabrication protocol has no high-temperature steps — as required for SiO_2 encapsulation and Bosch through-wafer etching, for example — the fabrication of the nickel nanomagnets is decoupled from almost all damage-inducing processing. Moreover, the serial-attachment protocol demonstrated here does not compromise the cantilever quality factor.

The concept of using FIB manipulation to attach a pre-prepared sample to a fragile, high-sensitivity cantilever can be extended to many other applications as well. Samples that require heat-intensive growing conditions such as carbon nanotubes[30] or samples that cannot tolerate the high-heat processing steps in cantilever fabrication such as superconducting rings[12] could all be adhered to cantilevers by this technique without extensive process integration challenges. This combination batch- and serial-fabrication process could also be used to attach a custom-fabricated magnetic tip onto the end of a commercial cantilever. Furthermore, FIB could be used to cross-section, liftout, and attach spin-cast samples onto the leading edge of cantilevers used in sample-on-cantilever MRFM experiments, which would significantly increase the number of available samples.[6]

Other key benefits of the magnet-tipped chip fabrication process arise from the flexibility of fabricating the magnets independently from the cantilevers. Since most damage-inducing chemical and heat-intensive processing steps were eliminated, switching the magnetic material from nickel to cobalt, which has a significantly higher saturation magnetization, should be straightforward. In contrast, Hickman *et al.* reported that cobalt was incompatible with the integrated magnet-on-cantilever protocol due to silicidation and etching by hydrofluoric acid.[16] Likewise, with some processing alterations, the magnetic material could also be switched to sputter-deposited permalloy or iron platinum, since any processing steps to remove the excess sputtered material such as chemical mechanical polishing or ion-beam milling would only damage the chips and not affect the quality factor of the high-compliance cantilevers. The magnet-tipped chip protocol also provides an ideal template for the incorporation of barrier layers. A substrate other than silicon could be implemented to prevent silicidation, such as SiO_2, silicon nitride, or tantalum. To prevent oxidation, ALD or other thin films could be blanket-deposited on the chips. This kind of blanket deposition could probably not be done on integrated cantilevers without significantly reducing the cantilever quality factor.

As described here, a magnetic chip must be attached to an independently fabricated cantilever to determine its magnetic moment. Further engineering of the magnetic chip to allow free oscillation would permit high throughput screening of potential magnetic nanorods without serial attachment. Such chips are also potentially much more sensitive of magnetic moment sensors than attonewton-sensitivity cantilevers because a shorter

cantilever is better optimized for high magnetic moment sensitivity such that the minimum detectable magnetic moment μ_{min} scales with $l^{3/2}$.[31]

The chip-on-cantilever protocol enabled the characterization of nanomagnet quality immediately after nickel deposition and on overhanging nanomagnets that had additional e-beam litography and isotropic plasma etching steps. The effects of adding a post-processing alumina oxidation barrier were also assessed. Cantilever frequency-shift magnetometry of 220 nm-wide magnets indicated that magnets were generally one-half to three-quarters magnetized, and that magnetization was unaffected by the fabrication steps required to produce both overhanging magnets and the oxidation barrier. Magnets that were 120 nm wide were less magnetized and ranged from roughly one-third to two-thirds magnetized. The decreased magnetization for smaller magnets is consistent with the presence of a uniform-thickness damage shell, since such a shell would consume a larger percentage of the smaller magnets.

The damage seen in the as-deposited nanomagnets is frankly puzzling. Both of the processing steps that were previously hypothesized as the sources of magnet damage — encapsulation with SiO_2 and Bosch through-wafer etching — were eliminated in the magnet-tipped chip protocol. Nickel oxidation seems unlikely since nickel oxide does not form in excess of 1 to 2 nm near room temperature and atmospheric pressure.[32–35] Damage due to silicide formation during the evaporation of hot nickel onto the substrate also seems unlikely, since the native oxide layer has been shown to be sufficient to prevent nickel silicidation.[36] An additional hypothesis is that the nickel reacted with the liftoff solvent CH_2Cl_2 during sonication. This hypothesis is not supported by energy dispersive X-ray spectroscopy (EDS) or electron energy loss spectroscopy (EELS) (data not shown), which showed no peaks corresponding to the presence of chlorine contamination on the magnets. The FIB attachment procedure also is not indicated to be a source of magnet damage. In addition to minimizing exposure to the gallium ions during processing, frequency shift cantilever magnetometry characterization was conducted on a seventh cantilever (C7 - data not included in Table I), which was coated with 10 nm of evaporated platinum in the same vacuum cycle as the nickel evaporation and had the same magnet dimensions as C1. The saturation magnetization of C7 was 0.37 ± 0.03 T, which is comparable to the other magnets with the same dimensions and indicates that coating with a protective layer does not reduce the damage to the magnet. Alternately, if the damage was due to ion-beam exposure at 30 kV, the maximum damage depth for gallium implantation would be approximately 30 nm, and a significant portion of the damage would be contained within the top 10 nm; in this case, a 10 nm protective coating of platinum should significantly reduce the damage. However, for completeness, a second test-case experiment should still be conducted in which the magnets are coated with at least 100 nm of platinum prior to FIB processing. In standard FIB processing for TEM sample preparation, the samples are coated with similar thick platinum layers to prevent gallium implantation. By determining the saturation magnetization of a magnet prepared by this method, the FIB attachment process would be completely eliminated as a damage source. Of course, a magnet with such a thick platinum layer could not be utilized in an MRFM experiment due to the significantly compromised tip-field gradient.

In order to develop magnets for sub-nanometer resolution proton imaging by NMR-MRFM, the magnetization loss seen here will need to be further mitigated, likely by optimizing magnetic material deposition. The yield of 50% to 75% magnetized tips has been improved from sub-1% to greater than 90%, and the protocol demonstrated here is well suited for rapid prototyping and analysis. The attonewton-sensivity cantilevers with overhanging magnetic nanorod tips shown in Fig. 3(f) can supply field gradients high enough for single-electron detection by ESR-MRFM, and could therefore be used to simultaneously localize

the positions of multiple nitroxide spin radicals on uniformly-labeled proteins to rapidly determine their tertiary structure.[4]

Acknowledgments

We acknowledge the National Institutes of Health (grant 5R01GM-070012), the Army Research Office MultiUniversity Research Initiative (grant W911NF-05-1-0403), and the National Science Foundation through the Cornell Center for Nanoscale Systems (grants EEC-0117770 and EEC-0646547). This work was performed in part at the Cornell NanoScale Science and Technology Facility, a member of the National Nanotechnology Infrastructure Network, which is supported by National Science Foundation (grant ECS-0335765). This work made use of the Transmission Electron Microscopy facility of the Cornell Center for Materials Research Science and Engineering Center (grant DMR-0520505).

References

1. Stowe TD, Yasumura K, Kenny TW, Botkin D, Wago K, Rugar D. Appl. Phys. Lett. 1997; 71:288.
2. Jenkins NE, DeFlores LP, Allen J, Ng TN, Garner SR, Kuehn S, Dawlaty JM, Marohn JA. J. Vac. Sci. Technol. B. 2004; 22:909.
3. Rugar D, Budakian R, Mamin HJ, Chui BW. Nature. 2004; 430:329. [PubMed: 15254532]
4. Moore EW, Lee S-G, Hickman SA, Wright SJ, Harrell LE, Borbat PP, Freed JH, Marohn JA. Proc. Natl. Acad. Sci. U.S.A. 2009; 106:22251. [PubMed: 20018707]
5. Garner SR, Kuehn S, Dawlaty JM, Jenkins NE, Marohn JA. Appl. Phys. Lett. 2004; 84:5091.
6. Degen CL, Poggio M, Mamin HJ, Rettner CT, Rugar D. Proc. Natl. Acad. Sci. U.S.A. 2009; 106:1313. [PubMed: 19139397]
7. Stowe TD, Kenny TW, Thomson DJ, Rugar D. Appl. Phys. Lett. 1999; 75:2785.
8. Kuehn S, Loring R, Marohn J. Phys. Rev. Lett. 2006; 96:156103. [PubMed: 16712172]
9. Yazdanian SM, Hoepker N, Kuehn S, Loring RF, Marohn JA. Nano Lett. 2009; 9:2273. [PubMed: 19435337]
10. Stipe BC, Mamin HJ, Stowe TD, Kenny TW, Rugar D. Phys. Rev. Lett. 2001; 86:2874. [PubMed: 11290061]
11. Ng TN, Jenkins NE, Marohn JA. IEEE Trans. Mag. 2006; 42:378.
12. Jang J, Budakian R, Maeno Y. 2010
13. Bleszynski-Jayich AC, Shanks WE, Ilic BR, Harris JGE. J. Vac. Sci. Technol. B. 2008; 26:1412.
14. Bleszynski-Jayich AC, Shanks WE, Peaudecerf B, Ginossar E, von Oppen F, Glazman L, Harris JGE. Science. 2009; 326:272. [PubMed: 19815772]
15. Choi J-H, Mirsaidov U, Miller C, Lee Y, Guchhait S, Chabot M, Lu W, Markert J. Proc. SPIE. 2004; 5389:399.
16. Hickman SA, Moore EW, Lee S-G, Longenecker JG, Wright SJ, Harrell LE, Marohn JA. ACS Nano. 2010; 4:7141. [PubMed: 21082863]
17. Brunner AJ, Ma E, Nicolet M-A. Appl. Phys. A. 1989; 48:229.
18. Panjan P, Kek Merl D, Zupanič F, Čekada M, Panjan M. Surf. Coat. Technol. 2008; 202:2302.
19. Beach E, Keefe M, Heeschen W, Rothe D. Polymer. 2005; 46:11195.
20. Grabulov A, Ziese U, Zandbergen H. Scripta Mater. 2007; 57:635.
21. Abolhassani S, Gasser P. J. Microsc. 2006; 223:73. [PubMed: 16872434]
22. Stevie FA, Vartuli CB, Giannuzzi LA, Shofner TL, Brown SR, Rossie B, Hillion F, Mills RH, Antonell M, Irwin RB, et al. Surf. Interface Anal. 2001; 31:345.
23. Langford RM, Petford-Long AK. J. Vac. Sci. Technol. A. 2001; 19:2186.
24. Marohn J, Fainchtein R, Smith D. Appl. Phys. Lett. 1998; 73:3778.
25. Ozatay O, Gowtham PG, Tan KW, Read JC, Mikhoyan KA, Thomas MG, Fuchs GD, Braganca PM, Ryan EM, Thadani KV, et al. Nat. Mater. 2008; 7:567. [PubMed: 18536721]
26. Zhang X, Zhao J, Whitney AV, Elam JW, Van Duyne RP. J. Am. Chem. Soc. 2006; 128:10304. [PubMed: 16881662]
27. Hanestad R, Butterbaugh JW, ben Hamida A, Gelmi I. Proc. SPIE. 2001; 4557:58.

28. Yazdanian S, Marohn J, Loring R. J. Chem. Phys. 2008; 128:224706. [PubMed: 18554042]
29. Aharoni A. J. Appl. Phys. 1998; 83:3432.
30. Chen I-C, Chen L-H, Orme CA, Jin S. Nano Lett. 2007; 7:3035. [PubMed: 17887798]
31. Ng, TN. Ph.D. thesis. New York: Cornell University; 2006.
32. Graham MJ, Cohen M. J. Electrochem. Soc. 1972; 7:879.
33. Kulpa SH, Frankenthal RP. J. Electrochem. Soc. 1977; 124:1588.
34. Pinnel MR, Tompkins HG, Heath DE. J. Electrochem. Soc. 1979; 126:1274.
35. Lambers ES, Dykstal CN, Seo JM, Rowe JE, Holloway PH. Oxid. Met. 1996; 45:301.
36. Lee P, Mangelinck D, Pey K, Ding J, Dai J, Ho C, See A. Microelectron. Eng. 2000; 51–52:583.

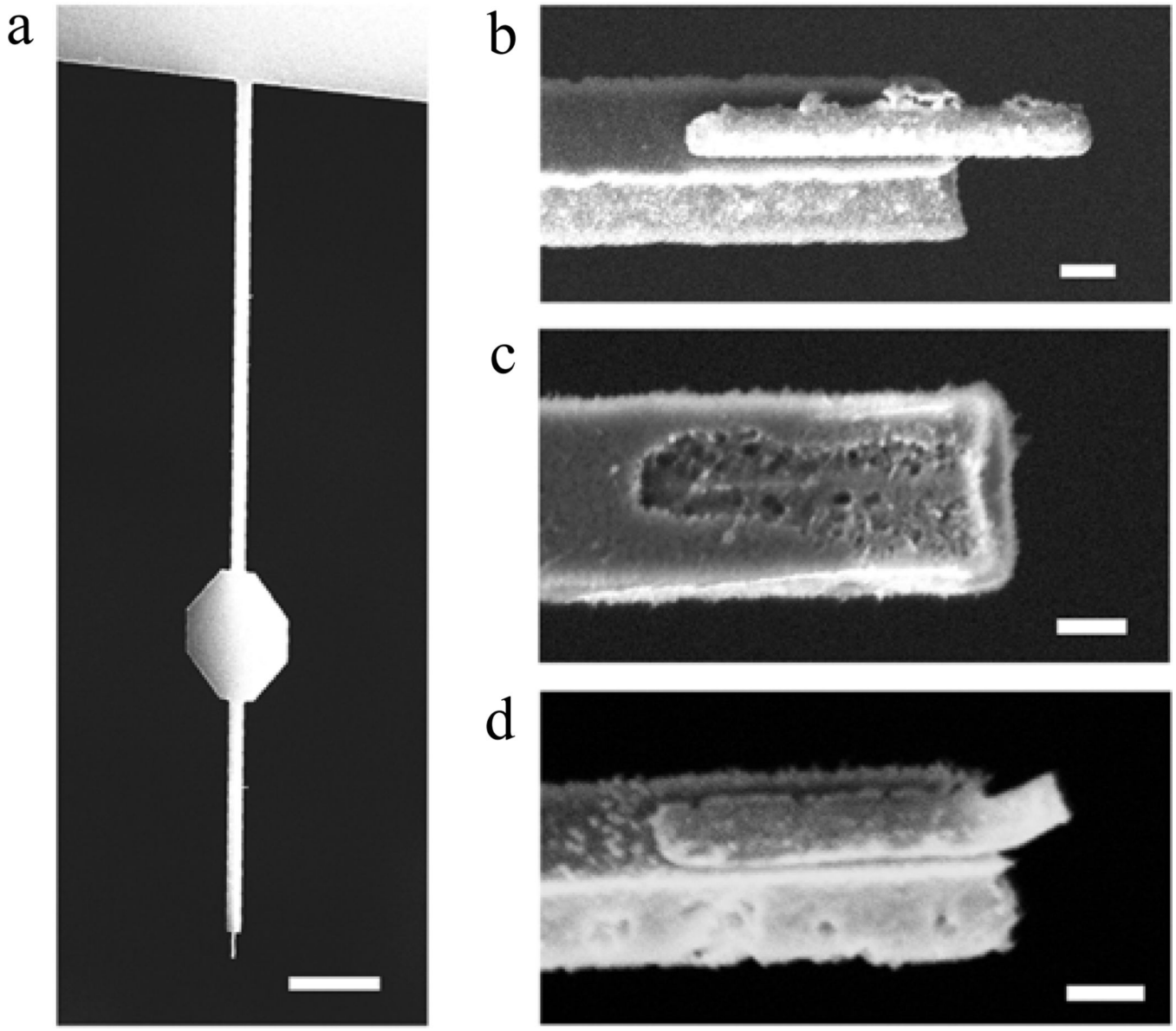

FIG. 1.

SEM images of post-processed magnets fabricated by a problematic batch fabrication approach, as outlined in Fig. 2 of Ref. 16. In this report we will discuss an alternative method that significantly improves the magnet yield. (a) The integrated magnets of Ref. 16 overhang the leading edge of 200 μm-long cantilevers. (b) Less than 1% of the fabricated magnets survived processing. Two common damage scenarios observed after processing were (c) complete magnet absence or (d) substantial magnet damage at the leading edge. The scale bar represents 20 μm in (a) and 200 nm in (b-d).

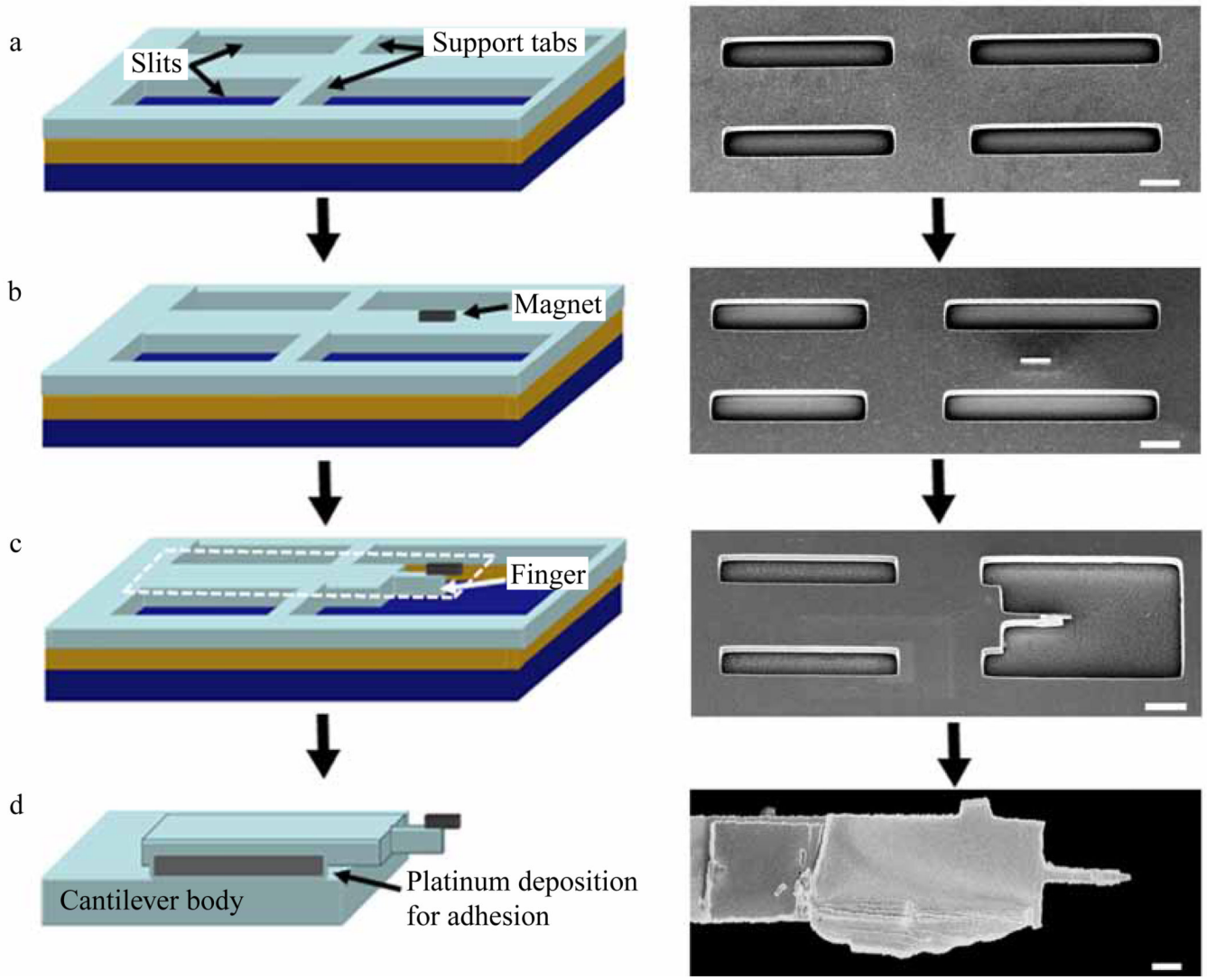

FIG. 2.

Process flow schematics (left) and corresponding SEM images (right) at key steps in the process used to fabricate overhanging magnet-tipped silicon chips and attach the chips to cantilevers. The magnet-tipped chips are fabricated by (a) etch slit definition and chip release, (b) magnet deposition, and (c) definition of the silicon leading-edge “finger”. To attach the chip to a cantilever, the portion of the chip inside the dashed line in the schematic in panel (c) is moved and attached to the leading edge of the cantilever (see text and Fig. 3), resulting in the magnet-tipped chip-on-cantilever shown in panel (d). From top to bottom, the layers in the schematics correspond to the nickel magnet (black), device silicon (light blue), buried silicion dioxide (yellow), handle silicon (dark blue), and ion-beam deposited platinum for adhesion of the chip to the cantilever (gray) (color online). Note that for ease of visualization, the SEM image in panel (c) has been processed by HF vapor release. For chips released prior to the silicon finger definition, handle-wafer silicon is also etched around the finger, as shown in Fig. 4(a). All scale bars are 2 μm.

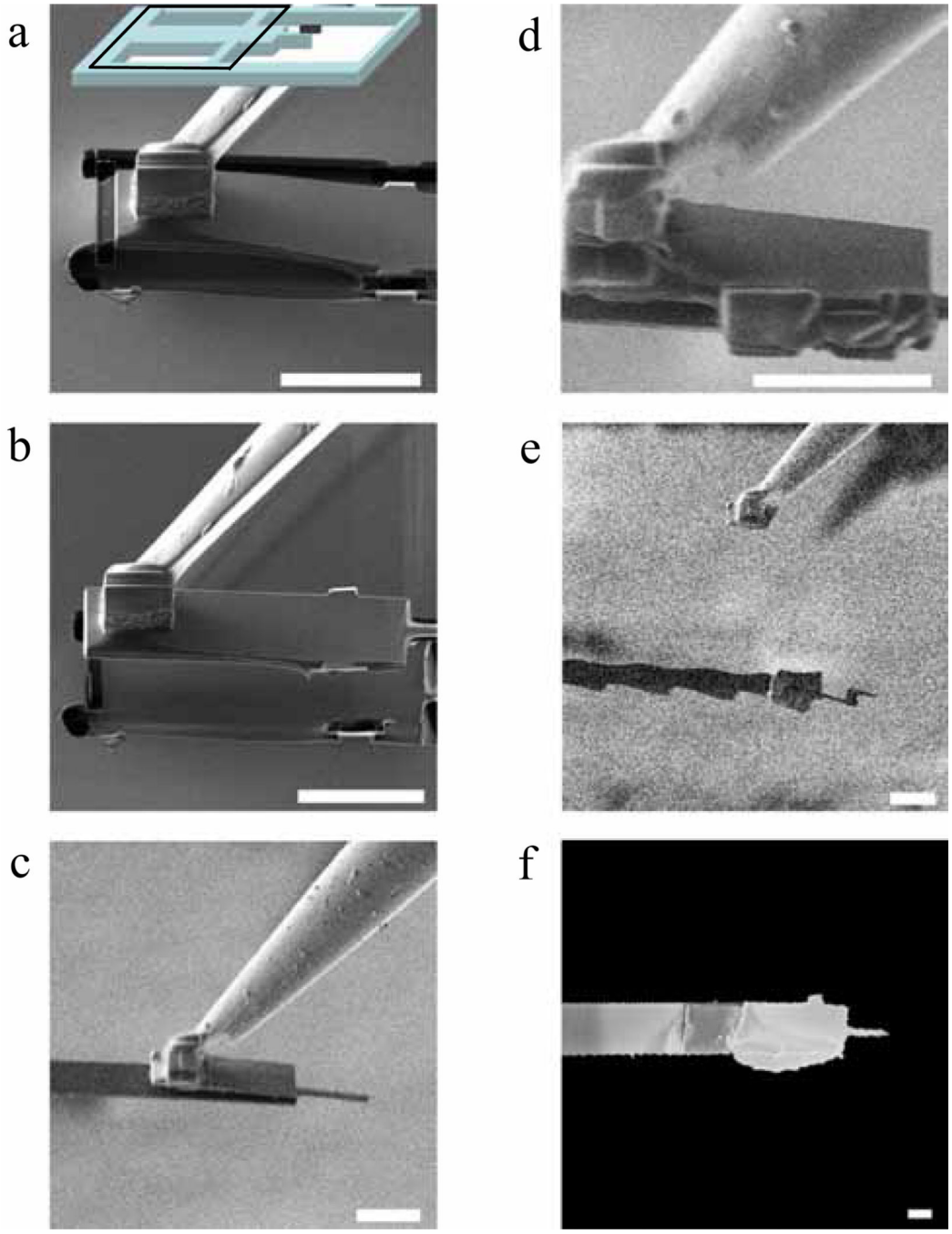

FIG. 3.

Ion-beam side-view (panels (a-e)) and SEM top-view (panel (f)) micrographs detail the magnet-tip liftout and cantilever-attachment procedure using a dual beam focussed-ion beam instrument. The inset in panel (a), which includes the chip device layer from Fig. 2(c), indicates the chip orientation and the box details the the visible region in the subsequent images. The process includes: (a) the probe tip is adhered to the magnet chip by FIB deposition of platinum; (b) the chip's support tabs are milled and the chip is lifted out; (c) the chip is positioned over the cantilever's leading edge and is brought into contact with the cantilever; (d) platinum deposition is used to adhere the chip to the cantilever; (e) the probe tip is milled and removed; and (f) the completed chip-on-cantilever. The serial attachment

process takes 1.5 hours per fabricated chip-on-cantilever assembly, with an additional 0.5 hour for sample loading and unloading from the chamber. All scale bars are 5 μm.

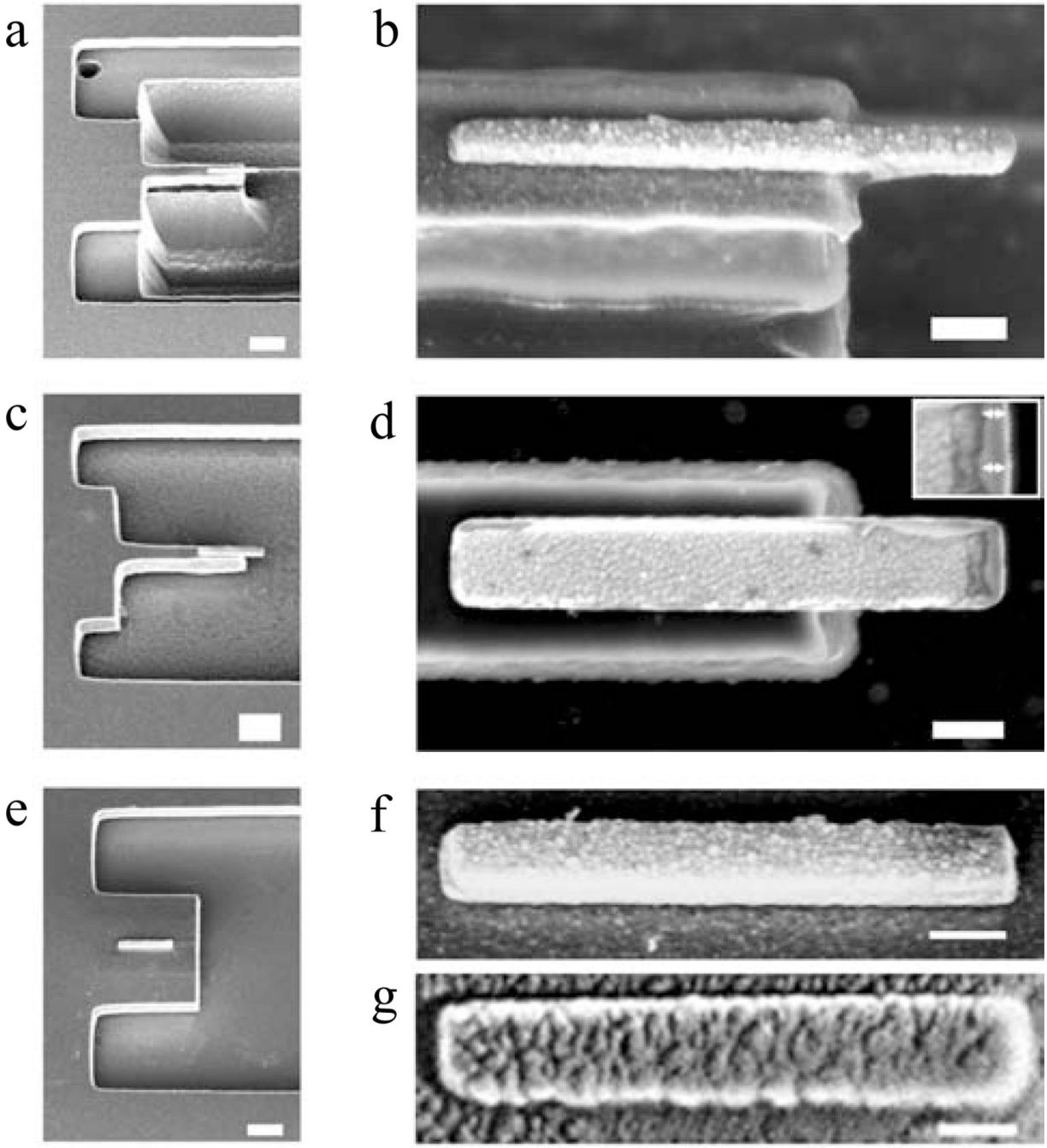

FIG. 4.

SEM images of the chip's leading edge (left) and corresponding magnified images of the associated magnets (right) produced by three release protocols: a chip with an overhanging nanomagnet, released prior to magnet deposition by a BOE wet etch (a, b); a chip with an overhanging nanomagnet, released by HF vapor after magnet deposition (c, d); and a chip with a non-overhanging magnet, released prior magnet deposition with a BOE wet etch (e-g). It can be seen in the inset in panel (d) that releasing with HF vapor damaged the magnet's leading edge; the arrows highlight the leading 20 nm of the magnet in which only the chromium adhesion layer is intact. The magnet in panel (g) is coated with approximately 6 nm of alumina prepared by atomic layer deposition. The magnets in panels (b) and (f) are

undamaged and uncapped. The scale bar in (a,c,e) is 1 μm. The scale bar in (b,d,f,g) is 200 nm.

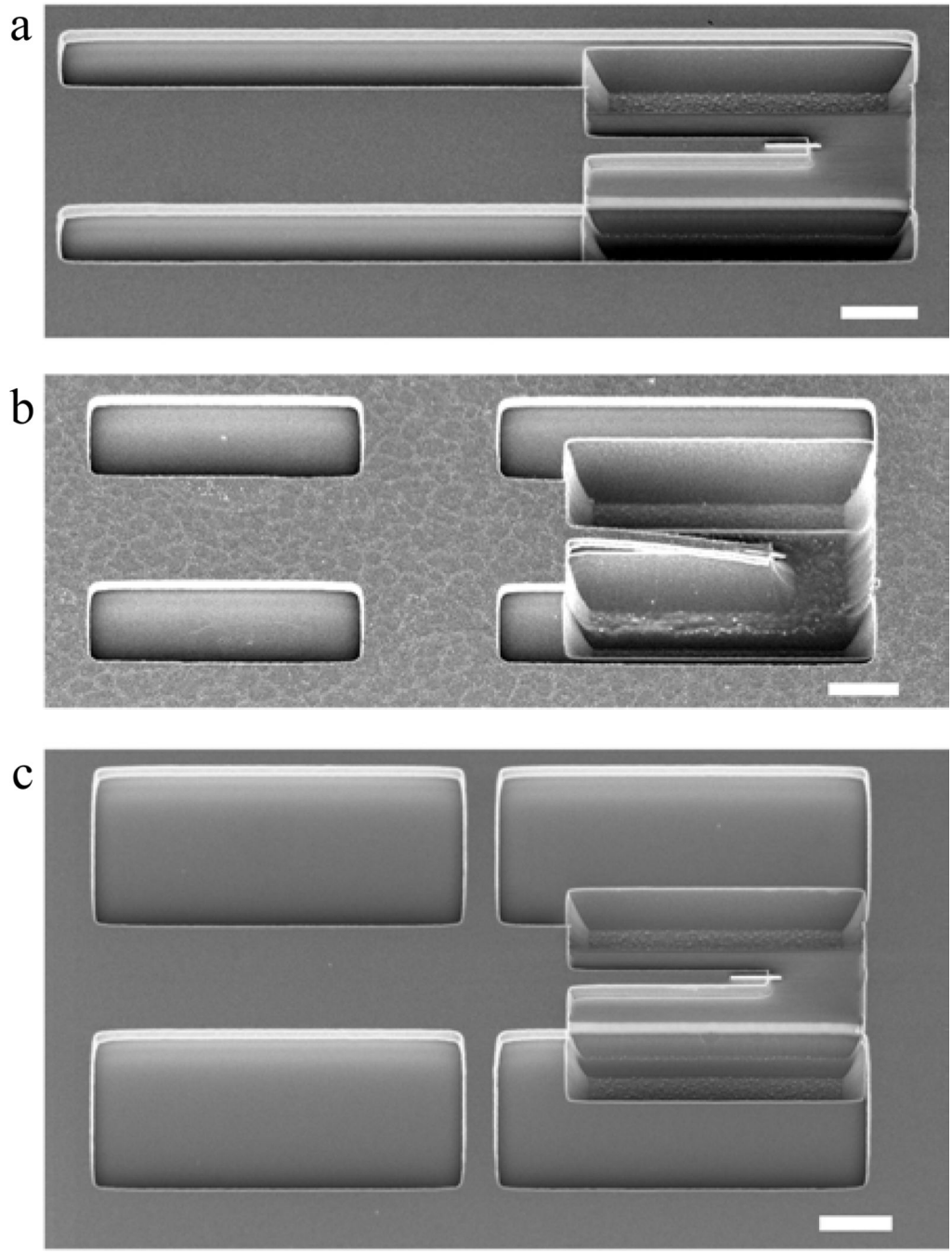

FIG. 5.

SEM images of unsuccessful alternative dimensions for the support tabs, slit widths, and silicon “finger” length. It was observed that (a) no support tabs, (b) long silicon fingers, and (c) wide slits and narrow support tabs all failed to prevent stiction-induced collapse of the leading finger supporting the tip’s overhanging magnet. For comparison, free-standing chips have an observable gap between the finger and the substrate, as shown in Fig. 4(a). All scale bars are 2 μm.

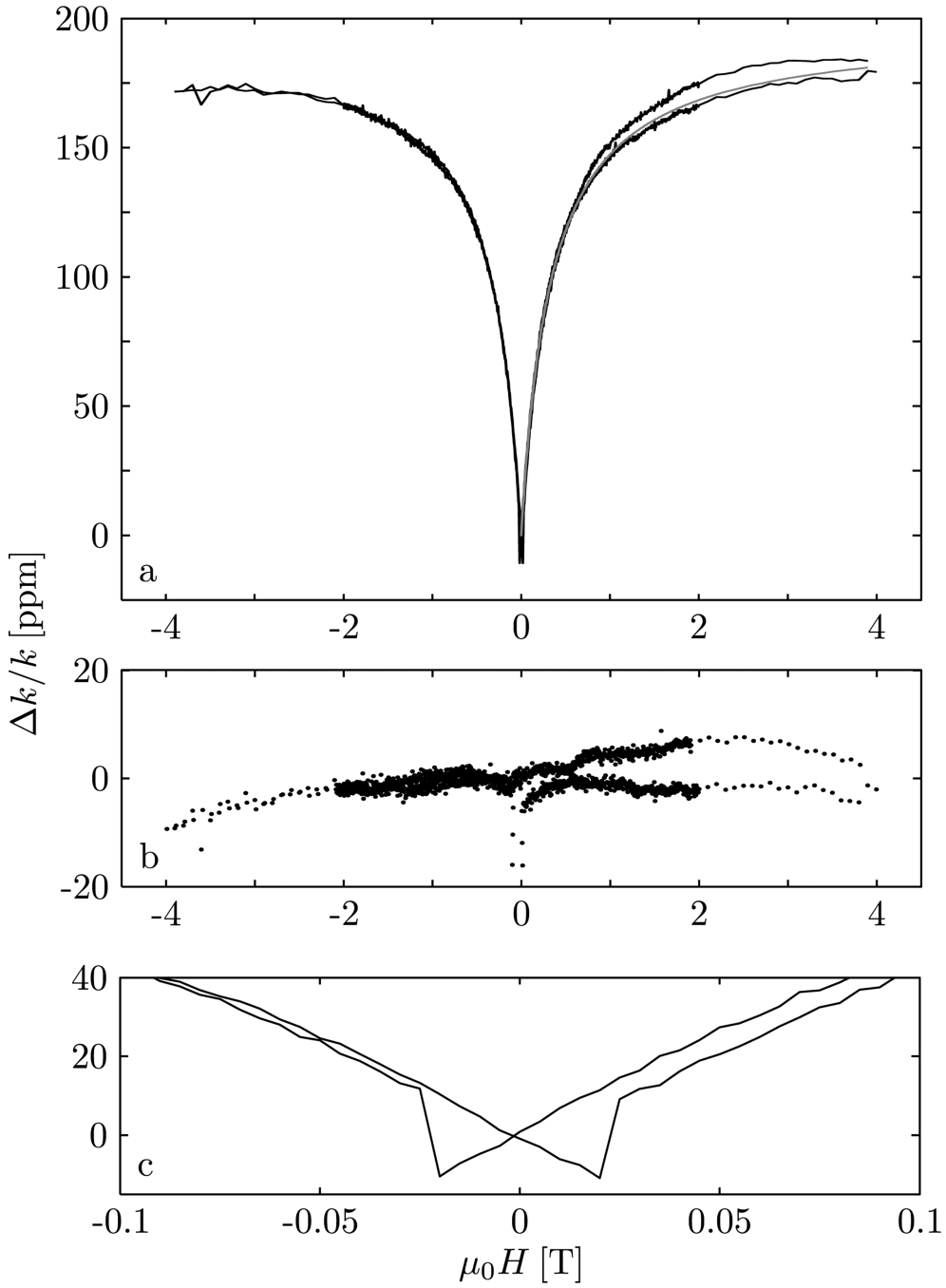

FIG. 6.

Easy-axis frequency-shift cantilever magnetometry for the 220nm-wide nickel nanomagnet on cantilever C1. Upper: data (solid; black) and best-fit to Eq. 1 (dotted; gray). Middle: fit residuals, shown for an applied field ranging from −4 T to +4 T. Lower: magnified view of the hysteresis present near zero field, indicating single-domain switching with a coercive field of H_c ~ 0.05 T.

TABLE I

Summary of cantilever and magnet properties. All values were measured at a field of 0 T unless otherwise indicated. All of the cantilevers studied had dimensions of 200 μm × 4 μm× 0.34 μm and unloaded resonance frequencies of $f_0 \approx 9000$ Hz.

quantity	C1	C2	C3	C4	C5	C6	unit
f_0	6631	6053	5054	6486	5351	4838	Hz
Q (at 0 T)	67,900	74,400	41,000	86,700	43,200	94,000	(unitless)
Q (at 5 T)	68,600	75,500	39,600	84,200	41,600		(unitless)
k	780	500	563 ± 63	780	780	703 ± 52	$\times 10^{-6}$ N m^{-1}
Γ	275	177	432	221	537	246	$\times 10^{-15}$ N s m^{-1}
F_{min}	8.0	6.4	10.0	7.2	11.2	7.6	$\times 10^{-18}$ N
l_m	1500	1500	1500	1500	1500	1500	nm
$l_{overhang}$	~300	~300	~300	~300	0	0	nm
w_m	220	120	120	220	220	220	nm
t_m	90	90	90	90	90	90	nm
$t_{Al_2O_3}$	0	0	0	0	5.6	5.6	nm
μ_{sat}	9.71 ± 0.98	4.50 ± 0.90	3.21 ± 0.30	9.08 ± 1.36	9.05 ± 1.43	11.72 ± 1.27	$\times 10^{-15}$ A m^{-2}
$\mu_0 M_{sat}$	0.41 ± 0.04	0.35 ± 0.07	0.25 ± 0.03	0.38 ± 0.06	0.38 ± 0.06	0.49 ± 0.08	T
ΔN	0.81 ± 0.08	0.51[a]	0.93 ± 0.10	0.99 ± 0.15	0.86 ± 0.15	0.40 ± 0.10	(unitless)
$\mu_{sat}^{nominal}$	14.18	7.73	7.73	14.18	14.18	14.18	$\times 10^{-15}$ A m^{-2}

[a] For this fit, ΔN was calculated from the magnet shape as described in the text.

J Vac Sci Technol B Nanotechnol Microelectron. Author manuscript; available in PMC 2012 October 01.